Wu et al. Int J Concr Struct Mater (2022) 16:52
https://doi.org/10.1186/s40069-022-00542-8

International Journal of Concrete Structures and Materials

RESEARCH Open Access

Structural Behavior Analysis of UHPC Hybrid Tower for 3-MW Super Tall Wind Turbine Under Rated Wind Load

Xiangguo Wu[1,2], Xuesen Zhang[3], Hom Bahadur Bhattarai[2*], Hyeon-Jong Hwang[4], Jing Yang[5] and Soonpil Kang[6*]

Abstract

Based on the conceptual design of an advanced wind turbine tower system, use of ultra-high-performance cementitious composites material with compressive strength of 200 MPa (UHPC-200) is proposed to ensure high durability and ductility of the UHPC hybrid wind turbine tower. Key design parameters are proposed for the structural design of a 3-MW wind turbine. The material properties, mixing compositions, simplified constitutive relationship, and model parameters are outlined. Using nonlinear finite element analysis, the effects of wall thickness, wall thickness ratio, and prestressing tendon on the structural performance including the longitudinal stress field, lateral displacement, stress concentration at the transition zone between the middle and bottom segments are evaluated. Based on the stress-field analysis, the design limitation of the segmental wall thickness and its ratio is recommended. The numerical results show that the tower with the wall thickness ratio of 2:3 (i.e., thickness 200–300 mm) with prestressing tendons is an optimal design for the UHPC hybrid tower. The results of this study can be used as a reference for the engineering design of a new type of UHPC hybrid wind turbine tower.

Keywords: wind turbine tower, UHPC, wall thickness, prestressing tendon, finite element analysis

1 Introduction

Developing renewable energy has been the main focus of many related institutions to cope with the ongoing climate crisis in recent times (IEA, 2019; Li et al., 2021). Along with other sources of clean and renewable energy, such as atomic, geothermal, solar, and hydraulic energy, the wind has played an essential role in energy production because of its vast potential to offer (Sadorsky, 2021). The commercial-scale rated turbine towers, with 10 to 50 kW up to 10 MW of power, require higher height and larger dimensions of support components to increase the size of turbine tower systems (Lana et al., 2021). Wind turbine towers need to be designed to place the power generation facilities at the optimal height to access a stable wind energy source, and strength, stiffness, and stability of tower sections are the important factors in the design (Pons et al., 2017). When the natural frequency of the tower structure matches with the rotational frequency of wind turbine blades and the blade-passing frequency, the resonance would result in the excessive deformation of the structure and consequently cause severe damage to it (Bernuzzi et al., 2021). In order to avoid such resonance, the tower frequency should range in between the blade-rotational frequency (1P) and blade-passing frequency (3P) or the soft–stiff range (CEC5008, 2018; LaNier, 2005). Furthermore, the requirement for high-rise structures limits the maximum deformation of the tower to be less than 1% of the

Journal information: ISSN 1976-0485 / eISSN 2234-1315

*Correspondence: 20sf33382@stu.hit.edu.cn; soonpil.kang.ks@nps.edu

[2] Key Lab of Structures Dynamic Behavior and Control of China, Ministry of Education, Harbin Institute of Technology, Harbin 150090, China
[6] Department of Applied Mathematics, Naval Postgraduate School, Monterey, CA 93943, USA
Full list of author information is available at the end of the article

total height of the structure (GB503135, 2019). In addition, the optimization of the shape and sizes of turbine tower structure is significantly important because the cost of the structure is about 20–30% of the overall price (Blanco, 2009; Jin & Li, 2019).

When the tower height exceeds 90 m, there are several obstacles that come to the manufacturing process for the steel section, such as the large thickness of over 40 mm, higher cost, and lower durability for fatigue and corrosion. Additionally, although the practical tower section diameter for highway transportation is limited to 4.5 m, larger segmental sizes are inevitable to produce the supporting structures of megawatt (MW) degree wind turbines (Quilligan et al., 2012). To bypass the highway transportation limitations and to develop durable and ductile tower structures, developing a hybrid tower with precast tapered section using cementitious material and short steel tapered conical part can be one of the promising design alternatives. Ultra-high-performance concrete (UHPC) is viable option of construction material for tower or mast structure due to its better performance in terms of fatigue and durability than normal concrete (Jammes & Cespedes, 2012). In this study, by implementing the concept of prefabricated UHPC segmental assembling technology and external prestressing system, the durability, ductility, and overall structure performance of a new generation of light-weight high-performance wind turbine tower structure are analyzed.

The UHPC material is formed by admixing short and thin steel fibers, high-strength cementitious matrix, and mineral admixtures with a special mixing technique and curing system (Fehling et al., 2014). UHPC exhibits high mechanical and durability properties with compressive strength in the range of 80–400 MPa, tensile strength ranging from 10 to 30 MPa, and elastic modulus of 40–50 GPa (Jing, 2013; Shafieifar et al., 2017). The superior performance of UHPC enables replacing the normal-strength concrete and high-strength concrete in future designs (Wu et al., 2009). Similarly, Soliman et al., (Soliman & Tagnit-Hamou, 2016) studied the mechanical and microstructural properties of a green ultra-high-performance glass concrete (UHPGC) with compressive strength up to 220 MPa, and observed that the properties were significantly improved when nonabsorptive glass-powder (GP) was used to replace the cement and quartz powder. Farzad et al. (Farzad et al., 2019) experimentally and numerically characterized the bond performance between concrete and overlaying regular concrete or UHPC layers. A review study by Li et al. (Hernandez-Estrada et al., 2019) and Matika et al. (Sritharan & Schmitz, 2013) showed that UHPC increases the strength and mass since UHPC barely contains water, chemical substances, and carbonation due to its low permeability and, therefore, corrosion of steel and alkali-silica reaction are retarded. This feature of UHPC also increases the relative dynamic modulus due to the accompanied freeze–thaw cycle effect. Such advantages enable UHPC to be used in severe environmental conditions. However, UHPC has not been frequently used in wind turbine tower structures, and further studies on various types of admixtures and cementitious materials are needed.

Hernandez-Estrada et al. (Hernandez-Estrada et al., 2019) provided a detailed review of loads actuating internal forces, techniques of structural analysis, widely used software, and some validation methods for implementation of a turbine tower. De Lana et al. (Lana et al., 2021) presented an optimization method to design structures of the tapered prestressed concrete tower and an octagonal tower by addressing the dynamic characteristics of the structures and using computer-aided engineering techniques and genetic algorithms. Sritharan et al. (Sritharan & Schmitz, 2013) presented a design alternative to conventional conical tower segments, using precast UHPC segments connected by high-strength bolts and post-tensioning tendons at the critical sections of turbine towers. Jammes et al. (Jammes & Cespedes, 2012) carried out a two-stage feasibility study of UHPC turbine tower where they adopted the finite element analysis based on the beam theory to design a global geometrical shape, and then employed shell elements to evaluate the local behavior of shells under service and ultimate load states. Recently, cementitious materials often supplanted steel in constructing precast concrete wind turbine towers to reduce the overall cost. The larger mass of the concrete towers has been a major technical issue, although they have the greater stiffness due to large thickness.

In the design of a super tall hybrid tower, the composition of wall thickness at each segment affects the overall structural response and stress distribution of the tower structure. Thus, in the present study, the effects of wall thickness, wall thickness ratio, and use of prestressing force on the structural behavior including the stress and lateral displacement distributions along the height of the super tall hybrid tower were investigated. The present study focuses on the static behavior of the structure by assuming that the natural frequencies of the structure are distanced from the rotor or blade-passing frequencies, thereby, the dynamic effects due to resonant interaction are minimal. Finite element analysis was performed to evaluate the structural behavior of the towers with the wall thickness ratio of 2:3 at the bottom and middle parts (i.e., 200–300 mm, 140–210 mm, and 100–150 mm in Fig. 1), and wall thickness ratio (i.e., 1:2, 2:3, and 5:6 with the thickness of 100–200 mm, 200–300 mm, and 200–240 mm, respectively). Based on the numerical results, a series of regression relationships between the structural

response and main design parameters were proposed for the preliminary design of tower. In conclusion, the UHPC turbine tower was recommended as a viable alternative for steel and normal-strength concrete tower based on the analysis results on the overall structural performance of H120 tower under rated wind speed.

2 Proposed Design for UHPC Hybrid Tower

This section provides an insight into the effects of the main technical parameters of 3 MW wind turbine system used in designing a high-performance hybrid tower structure. The details of design can be found in the literature (Engstroem et al., 2010). The tower is 120 m in height with three parts, including upper steel cylindrical segment, middle UHPC conical segment, and bottom UHPC tapered cylindrical part, as shown in Fig. 1. The upper steel cylindrical segment is 2 m in height with a wall thickness of 20 mm. The middle and bottom UHPC parts are 118 m in height in total, which are assembled by several prefabricated UHPC segments. The middle part has a clear height of 98 m, and its wall thickness varies from 100 to 200 mm. Its top surface is connected to the cylindrical steel segment. The height of the bottom tapered cylindrical segment is 20 m, and the local wall thickness varies from 150 to 300 mm. Every two parts are tied together using bolt connectors and external prestressing tendons at their interface (Fig. 1). Larger segments in the bottom and middle parts are subdivided into several UHPC longitudinal prefabricated segments to fulfill the width requirement for highway transportation.

The bottom part is composed of 4 segments, while the middle part is composed of 23 segments. The design height of 23 segments is uniformly 5 m. The adjacent segments are connected using flexible interval bolts. Each UHPC segment is formed along the rib ring, through which external prestressing tendons are perforated from the top to bottom. The diameters of the top and bottom of the tower are 3 and 12 m, respectively. Evenly spaced 12 holes are placed along the ring rib. Eight holes among them are filled by prestressing tendons, and six strands are arranged in each hole. The bolt connectors are placed at the remaining four holes.

3 Loads and Material Properties

The design loads on wind turbines include self-weight of tower, turbine weight, flexural moment due to the eccentricity of the top mass, horizontal thrust on wind wheel by wind, and the distributed wind load on tower (LaNier, 2005). It is noted that this study focuses on the load-carrying capacity and stress distribution of the tower structure under static loading.

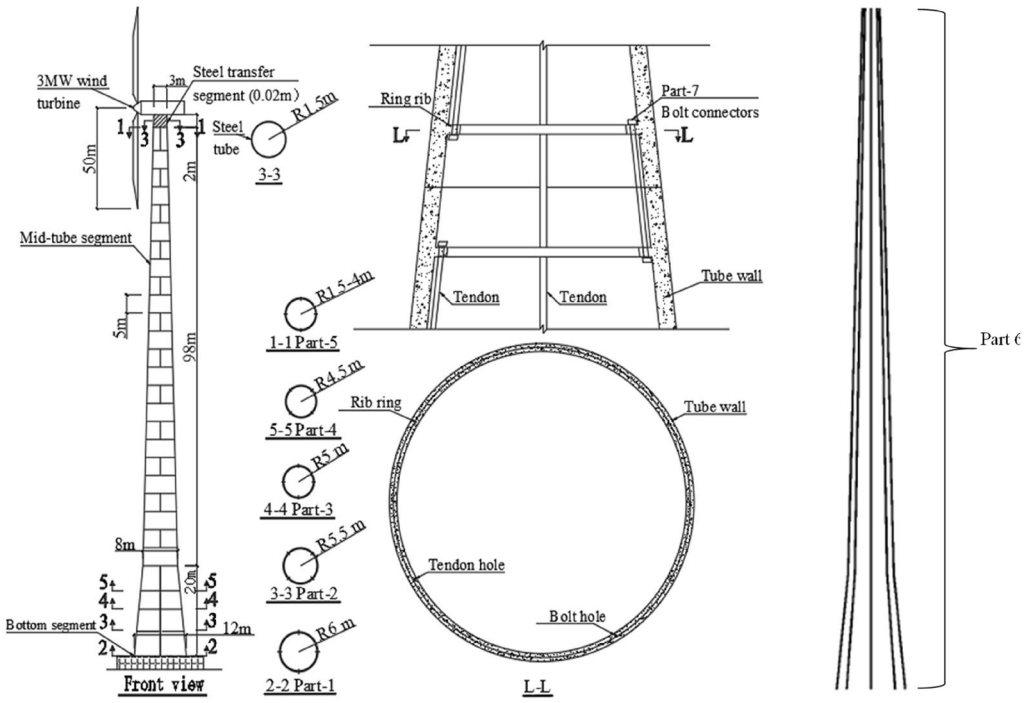

Fig. 1 Main part and detailed local diagram of the tower.

3.1 Design Parameters of Material

UHPC with compressive strength of 200 MPa, denoted as UHPC-200, is employed to design an ultra-high-performance hybrid turbine tower in this study. Detailed information of the mix proportion of UHPC-200 can be found in the literature (Wu et al., 2013), and the mixing technique and consecutive model of UHPC are presented in the literature (Wu et al., 2012).

According to the results of the uniaxial tensile test and cylinder splitting test, the tensile strength of the UHPC-200 increases to 25 MPa (Wu et al., 2013). For a simplified design, the value of the initial cracking strength is considered 6 MPa, which depends on design parameters, such as the volume ratio of steel fiber. The tensile strength of UHPC is approximately 6 to 8 times the tensile strength of the normal-strength concrete (NSC). The strain hardening effect of UHPC is neglected in this study.

Fig.2 shows the simplified stress–strain relationship of UHPC proposed by FHWA Report (Federal Highway Administration, 2006). The values of material properties are listed in Table 1. The material properties of prestressing tendons are listed in Table 2. Based on the wall thickness ratio of the tower, the analysis model is denoted as 200-300WTT, which indicates the analysis model having a wall thickness ratio of 200–300 mm.

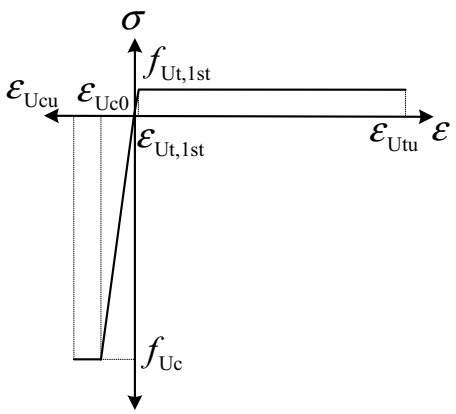

Fig. 2 Simplified stress–strain relation of UHPC.

Table 2 Properties of prestressing tendon.

Diameter of prestressing tendon	15.2 mm (1x7)
Ultimate tensile strength	1860 MPa
Density	7850 kg/m^3
Elastic modulus	1.95×10^5
Poisson's ratio	0.3
Prestressing stress	1231 MPa

3.2 Top Concentrated Load Under Rated Wind Speed

The wind turbine tower can be simplified as a cantilever beam with tapered cross-section according to the force analysis. The cantilever beam structure is subjected to distributed wind load, concentrated load at the top caused by the self-weight of engine room, hub, and nacelle, and the top concentrated moment caused by the eccentricity of the concentrated load (Zhao & Lv, 2009). As shown in Fig. 3a, the x-axis is the rotational axis of turbine wheel. The nacelle and turbine generator rotates with respect to z-axis. The y-axis is determined by the right-hand rule (Vorpahl & Popko, 2013).

In Fig. 3, F_x is the aerodynamic thrust on wind wheel, F_y is the pulsating force on the laminas, F_z is the axial compression force along the tower, M_x is the pitching moment due to the wind wheel and engine, M_y is the pitching moment resulted from the gradient of wind-load profile, and M_z is the torsion transferred from the wind wheel. The computed values for the concentrated loads at the top of the tower from the literature (Zhao & Lv, 2009) are summarized in Table 3.

The value of the wind design load on unit area of high-rise structures can be calculated following the guidelines (GB50135, 2019). The resulting value is equal to 222.8 N/m^2 for the hybrid tower under rated wind load.

4 Modeling of Hybrid Tower

A numerical analysis was performed on the UHPC hybrid tower structures with various wall thickness ratios at the bottom and middle segments. The geometric properties of the tower section are shown in Table 4. The finite element (FE) method was employed to model the tower structure, which was implemented using ABAQUS (Lee

Table 1 Parameters for the simplified constitutive model of UHPC.

Parameter	Tensile cracking strength ($f_{Ut,1st}$)	Tensile cracking strain ($\varepsilon_{ut,1st}$)	Ultimate tensile strength (f_{Utu})	Ultimate tensile strain (ε_{Utu})	Elastic modulus (E)	Poisson's ratio (μ)	Compressive strength (f_{Uc})	Ultimate compressive strain (ε_{Ucu})
Value	6–8 MPa	0.0001	15 MPa	0.0025	45 GPa	0.18	200 (MPa)	0.0036

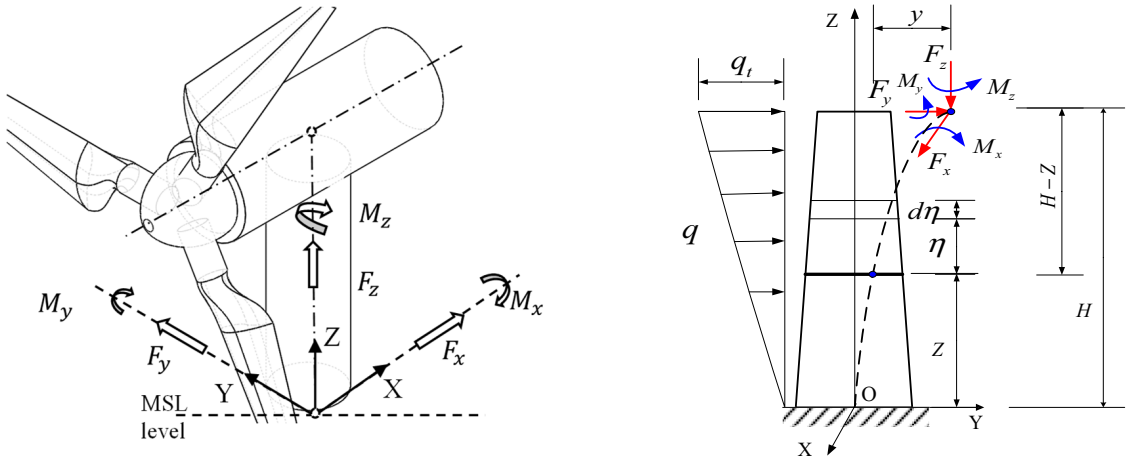

(a) Top concentrated loads **(b)** Simplified model of tower structure

Fig. 3 Coordinate system of tower.

Table 3 Loads on the top of the tower.

Loads	F_x (kN)	F_y (kN)	F_z (kN)	M_x (kNm)	M_y (kNm)	M_z (kNm)
	763.0	8.4	2077.6	4116.0	2376.5	282.3

Table 4 Geometric properties of the tower section.

Tower types	Tower top diameter (m)	Top cross-sectional area (m^2)	Tower base diameter (m)	Base cross-sectional area (m^2)
200-300WTT	3	2.545	12	11.02
140-210WTT	3	1.841	12	7.78
100-150WTT	3	1.343	12	5.58
200-240WTT	3	2.081	12	8.87
200-300WTT	3	2.545	12	11.02
100-200WTT	3	1.759	12	7.41

et al., 2020). First, the effect of wall thickness on the overall stress distribution of the UHPC tower was investigated using three tower models with the wall thickness range of 200–300 mm, 140–210 mm, and 100–150 mm (i.e., a fixed wall thickness ratio of 2:3). Second, the distribution of stress and deformation in the tower model was investigated according to wall thickness ratios (i.e., 1:2, 2:3, and 5:6, where the wall thickness was 100–200 mm, 200–300 mm, and 200–240 mm, respectively). Each section has 8 holes, and 6 equal prestressing tendons are placed at each hole. The total number of tendons is 48 at each section. The density of the tendon is 7850 kg/m^3, and the ultimate tensile strength is 1860 MPa. The coefficient for thermal expansion is 1.263×10^{-5}. The elastic modulus and Poisson's ratio are 195 GPa and 0.3, respectively. The controlled prestressed tensioning force of 1231 MPa (i.e., 0.65 f_{ptk}, which satisfies the code requirement of 0.7 f_{ptk} (GB50010, 2011)) is applied to the tendons.

The tower is divided into seven parts, in which parts 1 to 4 are the segments of the bottom part, and part 5 is the whole segment of the middle part. Prestressing tendons and prestressing bolts are numbered as part 6 and part 7, respectively. For finite element modeling, the UHPC parts 1 to 5 are discretized using three-dimensional four-node tetrahedral solid elements, while the prestressing bar parts 6 and 7 are discretized using the truss elements. The input values for the failure parameters of UHPC-200 are given in Table 5, which are the same as the default values of concrete plastic damage model in ABAQUS. In Table 5, Ratio 1 indicates the ratio of the ultimate biaxial compressive stress to the uniaxial compressive ultimate stress, Ratio 2 indicates the absolute value of the ratio of uniaxial tensile stress at failure to the uniaxial compressive stress at failure, Ratio 3 indicates the ratio of the magnitude of a principal component of plastic strain at ultimate stress in biaxial compression to the plastic strain at ultimate stress in uniaxial compression, and Ratio 4 indicates the ratio of the tensile principal stress value at cracking in plane stress, when the other nonzero

Table 5 Ratio of failure parameters for UHPC-200.

Ratio 1	Ratio 2	Ratio 3	Ratio 4
1.16	0.09	1.28	0.033

Table 6 Tension plasticity of UHPC-200.

$\sigma/f_{Ut,1st}$	1	1	0
$\varepsilon—\varepsilon_{Ut,1st}$	0	0.0024	0.0025

principal stress component is at the ultimate compressive stress value, to the tensile cracking stress under uniaxial tension. Table 6 lists the values for the plastic stress and strain in the damaged plasticity model that can be obtained from the simplified tension stress–strain model (Fig. 2), in which, $\sigma/f_{Ut,1st}$ is the ratio of the remaining stress to the tensile stress, and $\varepsilon—\varepsilon_{Ut,1st}$ is the residual of strain for the tensile strain.

The numerical analysis was performed in two steps (Lee et al., 2020). In the first step, the bars were prestressed in tension by means of the thermal strains created using the predefined temperature method. In the next step, the external loads were applied to the prestressed system. For modeling interactions of the segments, the tie constrain was imposed at the interface of the segments by assuming no tensile strain in concrete due to the prestressing. All the displacement components were fixed at the base during the loading. The gravity load, longitudinal distributed wind load, and concentrated loads at the top of the tower were applied to the tower. The concentrated loads include three components of the concentrated axial force and moments (Fig. 3). The mesh was generated using the methods of structured and sweep edges to consider the large dimension of the tower (Fig. 4) (Chen et al., 2014; Gu, 2009).

5 Analysis of the Tower Under Rated Wind Load

5.1 Effect of Wall Thickness

Fig. 5 compares the distribution of the longitudinal Mises stress on the windward and leeward sides of the tower in accordance with the wall thickness (i.e., towers 200-300WTT, 140-210WTT, and 100-150WTT with a fixed wall thickness ratio of 2:3). On the windward side, the similar patterns of stress distribution are observed in towers 140-210WTT and 200-300WTT, while the stress distribution in tower 100-150WTT deviates from the other two cases because of its lower stiffness (Fig. 5a). Because the tapered section decreased the inertia of the moment along the tower height, the tensile stress increased linearly along the tower height until 40 m, but it starts decreasing from 40 m height due to the effect of prestressing force. The tensile stress along the tower height in towers 140-210WTT and 200-300WTT nearly vanishes at around 100 m, and the compressive stress rapidly increased. In tower 100-150WTT, the boundary of the tension and compression zones lies around 60 m

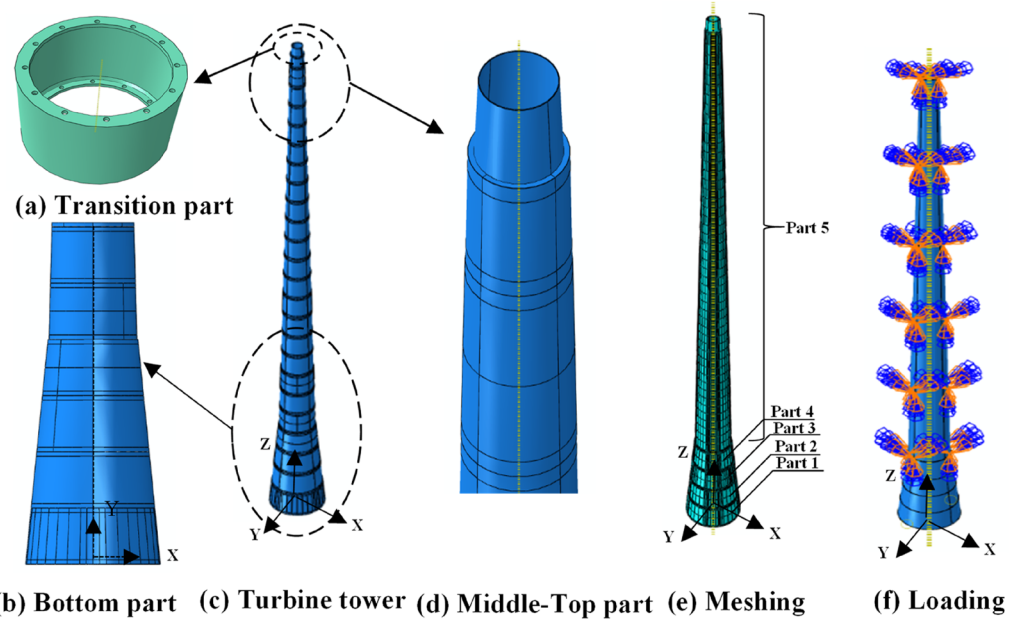

Fig. 4 Analysis model of the UHPC tower.

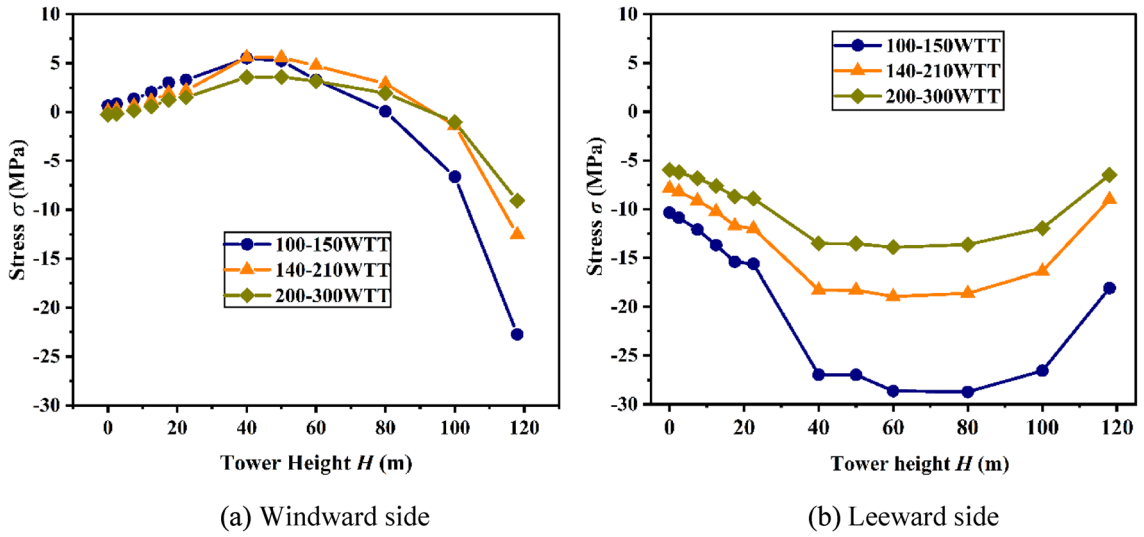

Fig. 5 Stress distribution of UHPC segment in towers with various wall thickness.

in height. The maximum tensile stress on the windward side was 5.25 MPa, which is within the range of tensile strength of the used UHPC material. Thus, the tensile crack would not occur on this side.

As shown in Fig. 5b, only compressive stress developed on the leeward side of the towers. The compressive stress increases linearly along with the height until 40 m along the tower height. The stress distribution between 40 and 100 m was relatively smooth. For towers 200-300WTT and 140-210WTT, the maximum compressive stress of about 13 and 20 MPa occurred in this region, respectively. The maximum compressive stress in tower 100-150WTT was about 30 MPa at the height of 80 m. The tower structure was in a compression state with its maximum value of about 30 MPa, which was significantly less than the compression strength of UHPC material. Thus, the compression failure would not occur in this test case. As the tower thickness increased, the tensile and/or compressive stress decreased.

Fig. 6 compares the lateral displacement of three tower models along with height. The maximum displacement occurred at the top for all tower models. The profiles of the lateral displacement depict the flexural behavior of the towers. As the wall thickness increased, the lateral displacement of the tower decreased. The lateral displacement was relatively small from the base to 50 m height in all the tower models, and increased significantly beyond the height of 50 m. Such result is attributed to the nonuniform load and stiffness along the height. The allowable deformation at the top of the tower is typically about 0.5–0.8% of the tower height, approximately 600–960 mm. The analysis results showed that the maximum

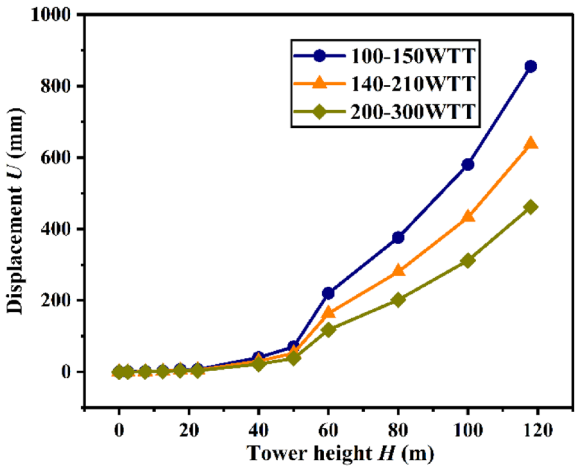

Fig. 6 Displacement distribution of UHPC segment in towers with various wall thickness.

lateral displacement of towers 100-150WTT, 140-210WTT, 200-300WWT were 855.1, 637.8, 461.4 mm at tower top, respectively, which satisfied the deformation requirement.

Fig. 7 shows the non-dimensionalized tensile stress (σ/f_{Utk}) and the non-dimensional lateral displacement ($u/u_{\max}$) on the windward side of the tower with various wall thicknesses, In this figures, σ is the maximum compressive stress; f_{Utk} is the specified tensile strength of UHPC (=6 MPa for UHPC-200); u is the lateral displacement at the tower top; and the $u_{\max}$ is the allowable lateral displacement at the tower top in design code

(GB50135, 2019). Based on the computed results, the regression curves of the tensile stress and lateral displacement are established as a function of the wall thickness in the tower with the wall thickness ratio of 2:3:

$$\frac{\sigma}{f_{\mathrm{Utk}}} = 1.725 - 0.0056t_{\mathrm{w}} \leq 0.933, \tag{1}$$

$$\frac{u}{u_{\max}} = 0.3356 - 0.0011t_{w}, \tag{2}$$

where t_{w} is the wall thickness in mm (= 100 to 200 mm in this study); and $u_{\max}$ is the maximal allowable lateral displacement (= 960 mm in this study).

5.2 Effect of Wall Thickness Ratio

To investigate the effect of wall thickness ratio, three tower models with different thickness ratios, 100-200WTT, 200-300WTT, and 200-240WTT, are chosen. Their wall thickness ratio is 1:2, 2:3, and 5:6, respectively. Fig. 8 compares the distribution of the longitudinal Mises stress on the windward and leeward sides of the towers.

On the windward side, the tensile stress linearly increased along with the height from the base to 40 m (Fig. 8a). In towers 200-300WTT and 200-240WTT, the tensile stress slightly decreased in the range of 40–80 m, and it became compressive stress at the height of about 80 m. In tower 100-200WTT, the maximum tensile stress was greater than 5 MPa, and the stress became compression at the height of 60 m. As the wall thickness ratio increased from 1:2 to 2:3, the tensile stress distribution at the windward side did not change significantly. However, when the wall thickness ratio increased from 2:3 to 5:6, the tensile stress decreased by 2.06 MPa at 40 m height.

As shown in Fig. 8b, the stress distribution on the leeward side was in compression through the height regardless of the wall thickness ratio. The compressive stress increased gradually until the height of 20 m, and rapidly increased between 20 and 40 m, particularly in tower 100-200WTT. The stress distribution was relatively smooth between 40 and 100 m where stress was governed by axial force rather than flexural moment. The maximum compressive stress occurred at the height of 60 m, which was less than 20 MPa. As the wall thickness ratio increased, the compressive stress at the leeward side decreased. The discrepancy of the maximum compressive stress between 1:2 and 5:6 wall thickness ratios was 5.03 MPa. This is because the smaller wall thickness decreases the stiffness, which increases the compressive stress.

Fig. 9 shows the lateral displacement along the height of the tower with various wall thickness ratios. The lateral displacement was relatively small below 50 m in height, and significantly increased in the upper region of the tower. The displacement curves of towers 200-300WTT and 200-240WTT were almost overlapping, and the maximum displacement was 461.4 and 450.9 mm, respectively, which satisfied the maximum allowable displacement of 960 mm. The displacement in tower 100–200 WTT was greater than that of the other towers, showing the maximum value of 830.4 mm, which was less than the allowable maximum deformation (i.e., 0.5–0.8% of the total height = 600–960 mm). It is noted that the tower wall thickness ratio does not significantly affect the displacement below 50 m, but it impacts on the top displacement of the towers.

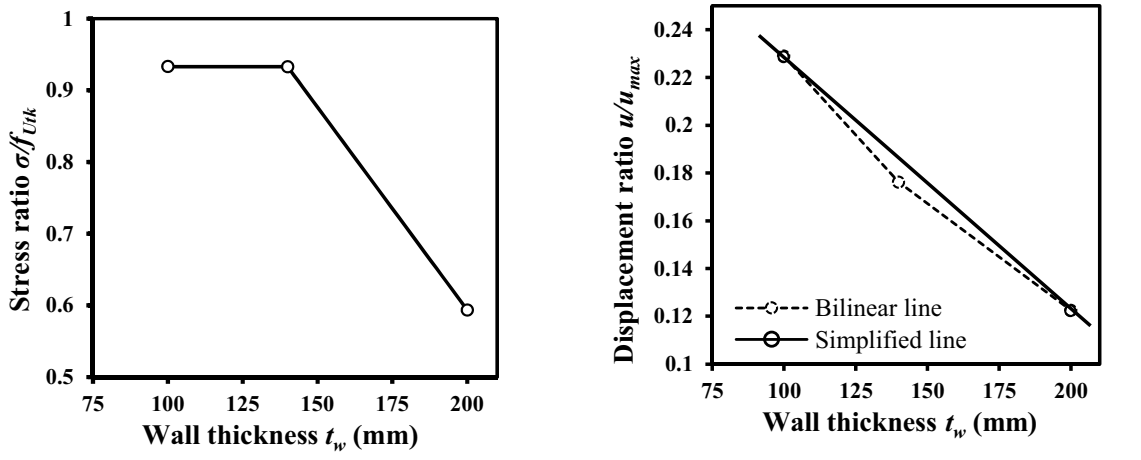

(a) Non-dimensionalized tensile stress **(b)** Non-dimensionalized lateral displacement

Fig. 7 Regression curves of the tensile stress and lateral displacement according to wall thickness.

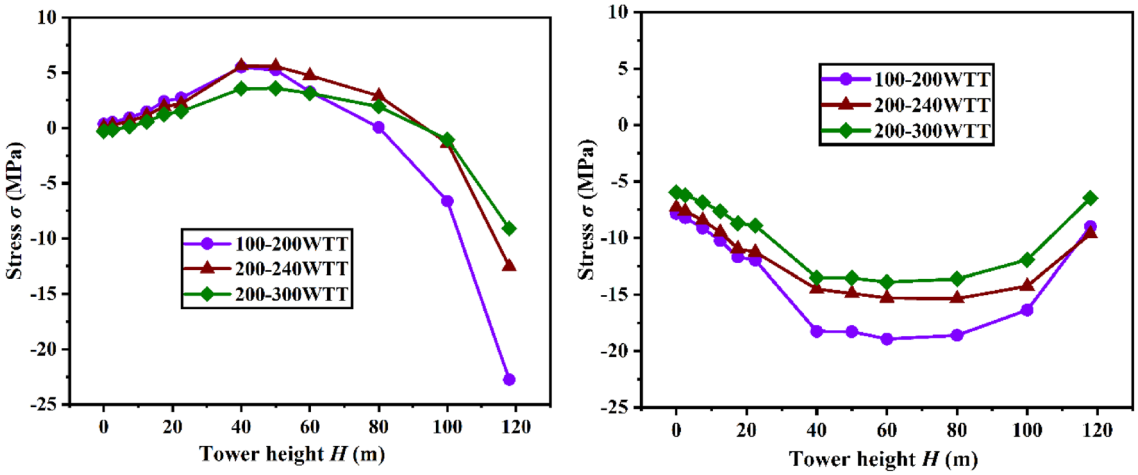

Fig. 8 Stress distributions of UHPC segment in towers with various wall thickness ratio.

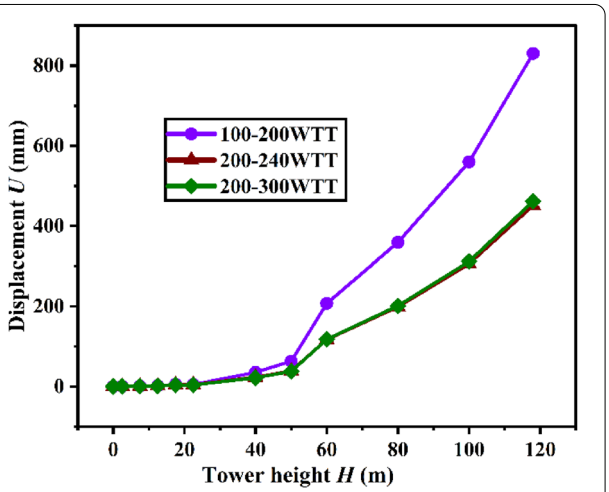

Fig. 9 Displacement distribution of UHPC segment in towers with various wall thickness ratio.

Fig. 10 shows the non-dimensionalized tensile stress (σ/f_{Utk}) and the non-dimensional lateral displacement ($u/u_{\max}$) on the windward side of the tower for various wall thickness ratios. Based on the computed results, the regression curves of the tensile stress and lateral displacement were established as a linear function of the wall thickness ratio:

$$\frac{\sigma}{f_{\mathrm{Utk}}} = 1.79 - 1.76R_w, \tag{3}$$

$$\frac{u}{u_{\max}} = 0.49 - 0.55R_w \geq 0.12, \tag{4}$$

where R_w is the wall thickness ratio (=0.5 to 0.83 in this study).

5.3 Effect of Prestressing Tendon

Figs. 11, 12 show the effect of prestressing force on the distributions of the longitudinal stress and lateral displacement in tower 200-300WTT that exhibits relatively low stress distribution and displacement. As shown in Fig. 11a, the maximum tensile stress in the tower without prestressing force was 12.4 MPa under the rated wind load, which was greater than the specified tensile strength of UHPC (i.e., 6 MPa). The prestressing force decreased the maximum tensile stress by more than 50%, while it increased the maximum compressive stress simultaneously. This result demonstrates that the prestressing force reduces the tensile stress effectively, which consequently improves the cracking resistance of the hybrid tower.

Fig. 12 compares the lateral displacement distribution in the towers with and without prestressing force. The lateral displacement was relatively small until the height of 50 m, and reached the maximum value of 461.8 mm at the height of 118 m. Regardless of the prestressing force, the displacement distribution was almost the same because the prestressing force contributed to shift the stress distribution but did not affect the cross-sectional stiffness. This result indicates that the effect of prestressing force on the lateral displacement is negligible because the lateral displacement is significantly affected by the cross-sectional stiffness. Thus, the prestressing force

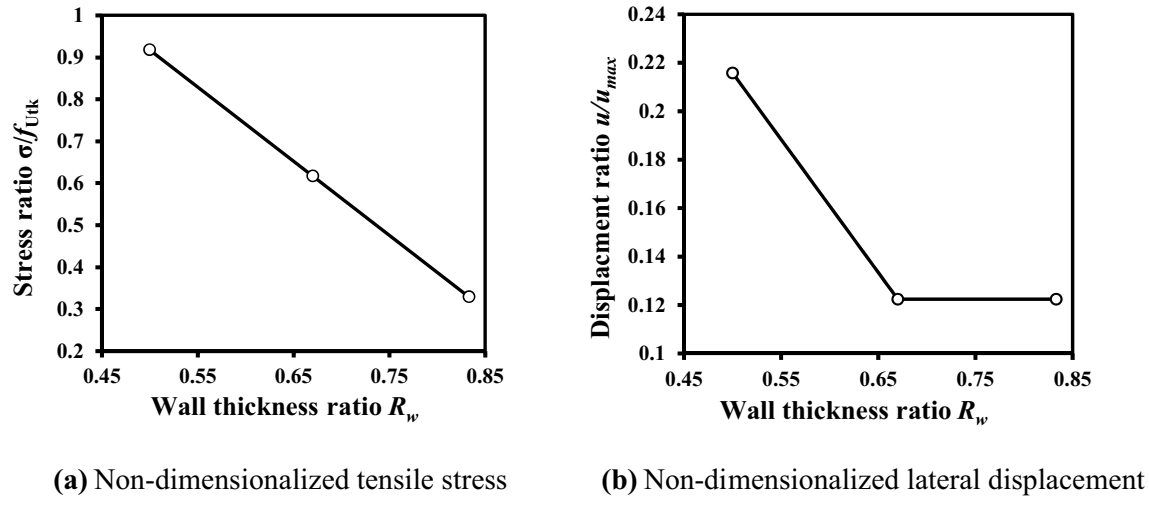

Fig. 10 Regression curves of the tensile stress and lateral displacement according to wall thickness ratio.

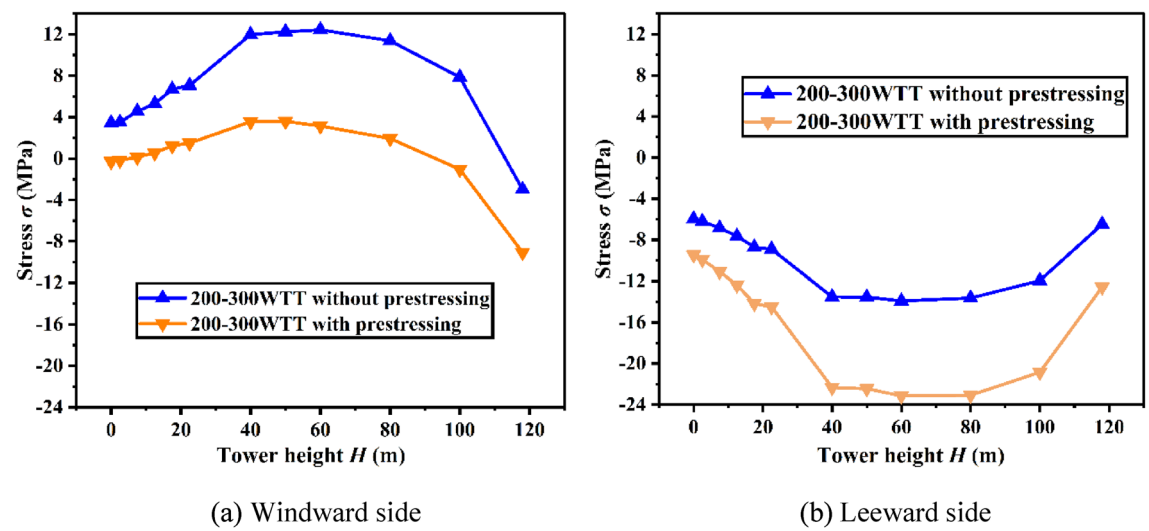

Fig. 11 Stress distribution of UHPC segment in towers with/without prestressing.

level needs to be determined from the section stress requirement.

To estimate the effect of the prestressing axial compression on the tensile stress of the section, a generic parameter t_wR_wn is introduced, in which, the axial compression ratio (n) is defined as follows:

$$n = \frac{f_{py}A_{ps}}{f_{Uc}A_U}, \tag{5}$$

where f_{py} is the yield strength of prestressing tendon; A_{ps} is the total cross-sectional area of the prestressing tendon; f_{Uc} is the design strength of UHPC (=95 MPa for UHPC-200); and A_U is the cross-sectional area corresponding to the maximum tensile stress zone (=5.53 m^2 for 200-300WTT with prestressing) at the height of 40–50 m (refer to Fig. 11a).

Fig. 13 shows the non-dimensionalized tensile stress (σ/f_{Utk}) in accordance with the wall thickness (t_w) in mm multiplied by wall thickness ratio (R_w) and axial compression ratio (n), and the non-dimensional lateral displacement (u/u_{max}) in accordance with the wall thickness (t_w) in mm multiplied by wall thickness ratio (R_w) as defined

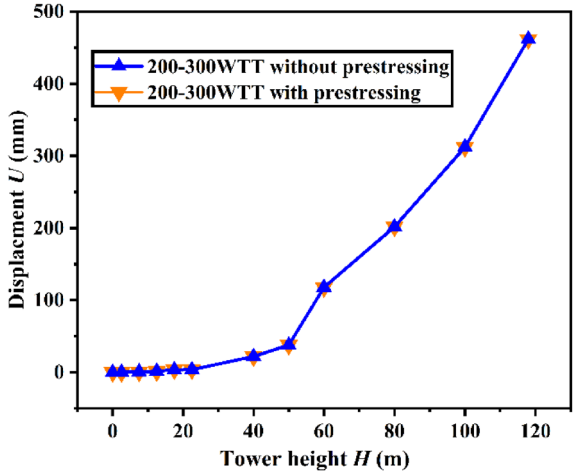

Fig. 12 Displacement distributions of UHPC segment in towers with and without prestressing.

in Eqs. (6, 7), respectively. When the t_wR_wn is greater than 1.58, σ/f_{Utk} is significantly decreased to 0.33 (Fig. 13a). Similarly, when t_wR_w is greater than 93.3, u/u_{max} significantly decreased to 0.12. It is noted that Eqs. (6, 7) can be used in the value of t_wR_wn from 0.85 to 2.82 and in t_wR_w from 50 to 167, respectively, in this study:

$$\frac{\sigma}{f_{Utk}} = 1.7 - 0.49t_wR_wn \le 0.933, \tag{6}$$

$$\frac{u}{u_{max}} = 0.37 - 0.002t_wR_w \le 0.23. \tag{7}$$

The approximation of the tensile stress in Eq. (6) can be used to check the tension limit as follows:

$$\frac{\sigma}{f_{Utk}} = 1.7 - 0.49t_wR_wn \le \frac{\sigma_{allow}}{f_{Utk}}, \tag{8}$$

where σ_{allow} is the allowable tensile stress. From the above relationship, the minimum requirement for n is obtained:

$$n = \frac{f_{py}A_{ps}}{f_{Uc}A_U} = \frac{f_{py}}{f_{Uc}}\rho_{ps} \ge \frac{3.47 - 2.04\sigma_{allow}/f_{Utk}}{t_wR_w}. \tag{9}$$

Finally, the minimum requirement for the prestressing–reinforcement ratio can be calculated by considering the allowable tensile stress:

$$\rho_{ps,min} = \frac{3.47 - 2.04\sigma_{allow}/f_{Utk}}{t_wR_w}\left(\frac{f_{Uc}}{f_{py}}\right). \tag{10}$$

6 Conclusions

The present study evaluated the effects of wall thickness, wall thickness ratio, and prestressing force on the structural behavior of a new-type ultra-high hybrid wind turbine tower. The distributions of the longitudinal stress and lateral displacement of the towers under various design parameters were investigated. The analysis results can be a reference for the implementation and engineering of new-type hybrid wind turbine towers. The primary findings can be summarized as follows:

(1) This study focused on a 3-MW wind turbine tower as a model tower. The 120-m tower structure is composed of several segments (23×5) of ultra-high-performance concrete (UHPC). Adjacent segments are tied using flexible interval bolts, and prestressing tendons perforate the segments with central ribs through the height. In a word, reinforcing bars are not used in the segments and connections. Only steel fibers are used in the segments, and prestressing tendons are used to connect the segments. The diameters of the top and bottom sections are 3 and 12 m, respectively. The concentrated force and moment of a wind turbine are applied to the tower top.

(2) The effect of wall thickness on the stress distribution and joint displacement: the maximum stress occurred at the height between 30 and 60 m. The maximum tensile stress in 100-200 mm and 200-240 mm towers reached the first cracking strength of UHPC-200. The leeward side of the towers was in the compression state. All types of towers exhibited larger compressive stress at middle height of the tower (40 to 100 m), and as the thickness increased, the compressive stress decreased significantly. Thus, thicker wall thickness at the middle height zone (40 to 100 m) enable to reduce the compressive stress considerably. Overall, the tower with the wall thickness of 200-300 mm exhibited lower compressive stress than the other typed towers.

(3) The effects of wall thickness ratio on the stress distribution and joint displacement: the stress distribution for all wall thickness ratios showed a similar pattern where the compressive and tensile stresses were maximized in the middle height. The effect of the wall thickness ratio on the displacement at the bottom part and the transition zone was negligible.

(4) The effects of prestressing force on the structural behavior: the prestressing force significantly decreased the tensile stress of the tower section, while preserving enough safety margin for the compressive stress. The tower without prestressing

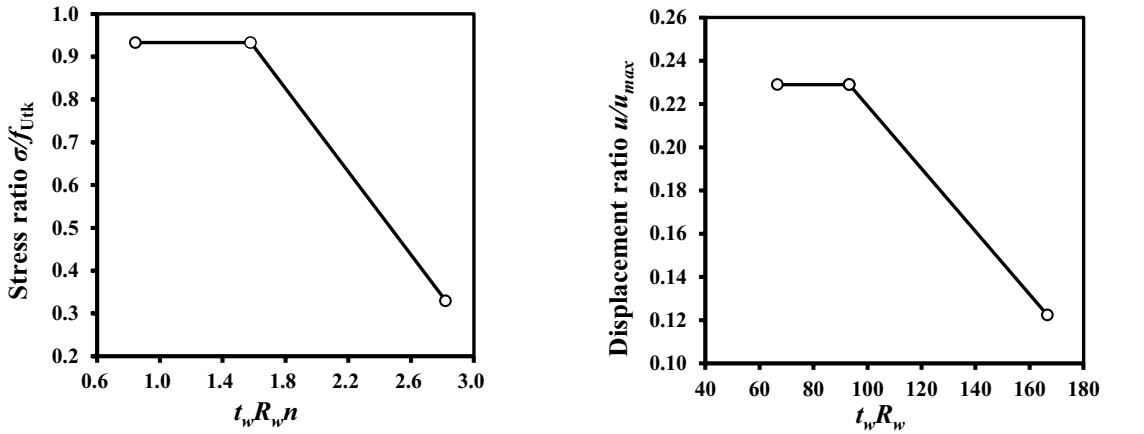

(a) Non-dimensionalized tensile stress **(b)** Non-dimensionalized lateral displacement

Fig. 13 Regression curves of the tensile stress and lateral displacement according to the wall thickness and wall thickness ratio.

exceeds the cracking strength of UHPC in the middle height from 40 m to 80 m.

(5) According to the overall evaluation of the analysis, the tower with the wall thickness ratio of 2:3 (i.e., thickness 200-300 mm) with prestressing tendons showed better structural performance than the other typed towers. Thus, this tower type is recommended for the practical implementation.

Authors' information
Xiangguo Wu is a Minjiang Scholar Professor in Fujian Provincial Key Laboratory of Multi-disasters Prevention and Mitigation in Civil Engineering, College of Civil Engineering at Fuzhou University(FZU), Fuzhou, China; a professor in Key lab of structures Dynamic Behavior and Control of China Ministry of Education at Harbin Institute of Technology(HIT), Harbin, China.
Xuesen Zhang is a Senior Engineer in CGN New Holdings Co., Ltd, Beijing, China; a Enterprise collaborative supervisor in College of Civil Engineering at Fuzhou University(FZU), Fuzhou, China.
Hom Bahadur Bhattarai is a Master candidate in Key lab of structures Dynamic Behavior and Control of China Ministry of Education at Harbin Institute of Technology(HIT), Harbin, China.
Hyeon-Jong Hwang is an Associate Professor in School of Architecture at Konkuk University, Seoul, Korea.
Jing Yang is a Senior Engineer in Harbin Power System Engineering and Research Institute of CNEEC Co., Ltd, Harbin, China.
Soonpil Kang is a Postdoctoral Research Associate at the Department of Applied Mathematics in Naval Postgraduate School supported by the National Academies of Sciences, Engineering, and Medicine, U.S.A.

Acknowledgements
The authors would like to thank the China National Natural Science Fund (52178195), the Xiamen Construction Science and Technology plan project (XJK2020-1-9), the open fund of Fujian Provincial Key Laboratory of Multi-disasters Prevention and Mitigation in Civil Engineering (College of Civil Engineering, Fuzhou University), and the Korea Agency for Infrastructure Technology Advancement (KAIA) grant funded by the Ministry of Land, Infrastructure and Transport (Grant No. 1615012146) for the support to the authors' work described herein.

Author contributions
XW: conceptualization, methodology, writing—original draft preparation, project administration. XZ: conceptualization, methodology, supervision. HBB: data curation, FEM modeling and parameter analysis. HJH: conceptualization, methodology, supervision. JY: data curation and parameter analysis. SK: writing—review and editing. All authors read and approved the final manuscript.

Funding
The funding sources are presented in acknowledgements.

Availability of data and materials
The data presented in this study are available on request from the corresponding authors.

Declarations

Ethics approval and consent to participate
Not applicable.

Consent for publication
The authors consent for publication.

Competing interests
The authors declare that they have no known competing financial interests or personal relationships that could have appeared to influence the work reported in this paper.

Author details
[1]Fujian Provincial Key Laboratory of Multi-Disasters Prevention and Mitigation in Civil Engineerings, College of Civil Engineering, Fuzhou University, Fuzhou 350108, China. [2]Key Lab of Structures Dynamic Behavior and Control of China, Ministry of Education, Harbin Institute of Technology, Harbin 150090, China. [3]CGN New Holdings Co, Ltd, Beijing 100070, China. [4]School of Architecture, Konkuk University, Seoul 05029, South Korea. [5]Harbin Power System Engineering and Research Institute of CNEEC Co, Ltd, Harbin, China. [6]Department of Applied Mathematics, Naval Postgraduate School, Monterey, CA 93943, USA.

Received: 25 April 2022 Accepted: 19 June 2022
Published online: 03 October 2022

References

Bernuzzi, C., et al. (2021). Resonance of steel wind turbines: problems and solutions. *Structures, 32*(March), 65–75. https://doi.org/10.1016/j.istruc.2021.02.053

Blanco, M. I. (2009). The economics of wind energy. *Renewable and Sustainable Energy Reviews, 13*(6–7), 1372–1382. https://doi.org/10.1016/j.rser.2008.09.004

Chen, W., Wang, S. Y., Cao, L., Wang, H. M., & Yao, J. (2014). The finite element analysis of the large horizontal axis wind turbine generator tower. *Applied Mechanics and Materials, 444–445*, 836–840. https://doi.org/10.4028/www.scientific.net/AMM.444-445.836

China electricity council T / CEC 5008-2018, Code of prestressed precast concrete tower for wind turbine. 2018.

GB 50135-2019, Standard for design of high-rising structures. 2019.

de Lana, J. A., Júnior, P. A. A. M., Magalhães, C. A., Magalhães, A. L. M. A., de Andrade Junior, A. C., & de Barros Ribeiro, M. S. (2021). Behavior study of prestressed concrete wind-turbine tower in circular cross-section. *Engineering Structures*. https://doi.org/10.1016/j.engstruct.2020.111403

Engstroem, S., Lyrner, T., Hassanzadeh, M., Stalin, T., & Johansson, J. (2010). Tall towers for large wind turbines. Report from Vindforsk project V-342, Sweden, 1-49. https://fdocuments.net/document/tall-towers-for-large-wind-turbines-ostigov.html?page=1

Farzad, M., Shafieifar, M., & Azizinamini, A. (2019). Experimental and numerical study on bond strength between conventional concrete and ultra high-performance concrete (UHPC). *Engineering Structures, 186*, 297–305. https://doi.org/10.1016/j.engstruct.2019.02.030

Federal highway administration, "Structural behavior of ultra-high performance concrete prestressed I-Girders,".106, 2006. http://www.tfhrc.gov/structur/pubs/06115/index.htm

Fehling E, Schmidt M, Walraven J, et al. (2014). Ultra-High Performance Concrete UHPC, Fundamentals, Design, Examples. Ernst & Son.

GB 50010–2010, "Code for design of concrete structures," 2011.

Gu F. (2009), The research of Steel-Concrete Hybrid Tower of the wind turbine (D), Xinjiang Agricultural University, 14-15.

Hernandez-Estrada, E., et al. (2019). Considerations for the structural analysis and design of wind turbine towers: a review. *Renewable and Sustainable Energy Reviews, 137*(December), 2021. https://doi.org/10.1016/j.rser.2020.110447

IEA (2019), World Energy Outlook 2019. www.iea.org/weo%0Ahttps://www.iea.org/reports/world-energy-outlook-2019%0Ahttps://www.iea.org/reports/world-energy-outlook-2019%0Ahttps://webstore.iea.org/download/summary/2467?fileName=Japanese-Summary-WEO2019.pdf

Jammes F, & Cespedes X. (2012). Design of UHPC Wind Turbines, Innovative Infrastructures – Towards Human Urbanism, 18th IABSE Congress, 1049–1056. https://doi.org/10.2749/222137912805111546

Jin, Q., & Li, V. C. (2019). Structural and durability assessment of ECC/concrete dual-layer system for tall wind turbine towers. *Engineering Structures, 196*, 109338. https://doi.org/10.1016/j.engstruct.2019.109338

Jing, Y. (2013). Ultra high UHPC - steel hybrid wind turbine tower structure performance using numerical simulation. Harbin Engineering University. https://kns.cnki.net/KCMS/detail/detail.aspx?dbname=CMFD201401&filename=1014132891.nh.

LaNier, M. W. (2005). LWST Phase I Project Conceptual Design Study: Evaluation of Design and Construction Approaches for Economical Hybrid Steel/Concrete Wind Turbine Towers; June 28, 2002 -- July 31, 2004". United States. https://doi.org/10.2172/15011444

Lee, S. H., Abolmaali, A., Shin, K. J., & Du Lee, H. (2020). ABAQUS modeling for post-tensioned reinforced concrete beams, *Journal of Building Engineering, 30*, 101273. https://doi.org/10.1016/j.jobe.2020.101273

Li, M., Hamawandy, N. M., Wahid, F., Rjoub, H., & Bao, Z. (2021). Renewable energy resources investment and green finance: evidence from China. *Resources Policy, 74*, 102402. https://doi.org/10.1016/j.resourpol.2021.102402

Pons, O., De La Fuente, A., Armengou, J., & Aguado, A. (2017). Towards the sustainability in the design of wind towers. *Energy Procedia, 115*, 41–49. https://doi.org/10.1016/j.egypro.2017.05.005

Quilligan, A., O'Connor, A., & Pakrashi, V. (2012). Fragility analysis of steel and concrete wind turbine towers. *Engineering Structures, 36*, 270–282. https://doi.org/10.1016/j.engstruct.2011.12.013

Sadorsky, P. (2021). Wind energy for sustainable development: Driving factors and future outlook. *Journal of Cleaner Production, 289*, 125779. https://doi.org/10.1016/j.jclepro.2020.125779

Shafieifar, M., Farzad, M., & Azizinamini, A. (2017). Experimental and numerical study on mechanical properties of ultra high performance concrete (UHPC). *Construction and Building Materials, 156*, 402–411. https://doi.org/10.1016/j.conbuildmat.2017.08.170

Soliman, N. A., & Tagnit-Hamou, A. (2016). Development of ultra-high-performance concrete using glass powder—towards ecofriendly concrete. *Construction and Building Materials, 125*, 600–612. https://doi.org/10.1016/j.conbuildmat.2016.08.073

Sritharan, S., & Schmitz, G. M. (2013). Design of tall wind turbine towers utilizing UHPC, *RILEM-fib-AFGC Int. Symp Ultra-High Perform Fibre-Reinforced Concr, 1*, 433–442.

Vorpahl, F., & Popko, W. (2013). *Description of the Load Cases and Output Sensors to be Simulated in the OC4 Project under IEA Wind Annex 30* (p. 23). Bremerhaven, Germany: Fraunhofer Institute for Wind Energy and Energy System Technology IWES.

Wu, X. G., Xu, S. L., & Wu, M. X. (2009). Fracture parameters study and application of ultra high performance fiber reinforcement concrete. *Gongcheng Lixue/engineering Mechanical, 26*(3), 93–98.

Wu, X., Yang, J., & Mpalla, I. B. (2013). Preliminary design and structural responses of typical hybrid wind tower made of ultra high performance cementitious composites. *Structural Engineering and Mechanics, 48*(6), 791–807. https://doi.org/10.12989/sem.2013.48.6.791

Wu, X. G., Zhao, X. Y., & Han, S. M. (2012). Structural analysis of circular UHPCC form for hybrid pier under construction loads. *Steel Composite Structures, 12*(2), 167–181. https://doi.org/10.12989/SCS.2012.12.2.167

Zhao, R. Z., & Lv, G. (2009). "Static analysis of the tower for horizontal wind turbine based on finite element", compressor. *Blower Fan Technol, 4*, 83.

Publisher's Note